



IIT MADRAS

FINAL YEAR BTECH PROJECT

Lattice Boltzmann simulation of evaporating droplet

Aqel Ahammad K P
CH13B006

Guided by
Prof. Sumesh Thampi

May 8, 2017

Contents

1	Abstract	1
2	Governing equations	1
3	Lattice-Boltzmann method	1
4	LB Method and Method of Lines	1
5	Spinodal decomposition	2
6	Surface tension	3
7	Variation of phase field close to interphase	3
8	Solid wall	4
9	Evaporation of a planar droplet	4
10	Condensation of planar droplet	4
11	Evaporation and condensation of a sessile droplet on a solid surface	5
11.1	Ideal surface	5
11.2	Hysteretic surface	6
12	Discussion and Conclusions	7
13	Future work	9

1 Abstract

Evaporation and condensation is modeled in this study using two methods - Lattice Boltzmann method and Method of lines. These two methods were evaluated based on space and time complexity, average time for one iteration and time for convergence. Evaporation of planar droplet was simulated and reproduced results mentioned in the literature. The boundary condition for evaporation was reversed for initiating condensation and was able to bring opposite effect. Evaporation and condensation of a sessile droplet was studied on ideal and hysteretic surfaces. The results showed same pattern that is recorded experimentally. Pinning of contact line during evaporation was achieved on a hysteretic surface by defining a smaller receding angle.

2 Governing equations

Continuity equation,

$$\frac{\partial \rho}{\partial t} + \nabla \cdot (\rho \vec{v}) = 0 \quad (1)$$

Navier-Stokes equation,

$$\rho[\vec{v} + (\vec{v} \cdot \nabla) \vec{v}] = \eta \nabla^2 \vec{v} - \phi \nabla \mu - \nabla P \quad (2)$$

Cahn-Hilliard convection-diffusion equation,

$$\frac{\partial \phi}{\partial t} = \nabla \cdot (\phi \vec{v}) + \nabla \cdot (M \nabla \phi) \quad (3)$$

where ϕ is the phase field and M is *mobility parameter* which plays the role of diffusivity.

3 Lattice-Boltzmann method

Instead of solving equations (1)-(3), the discrete Boltzmann equation is solved to simulate the flow of a Newtonian fluid.

$$f_i(\mathbf{r} + \mathbf{c}_i \Delta t, t + \Delta t) - f_i(\mathbf{r}, t) = -\frac{\Delta t}{\tau} (f_i - f_i^{eq}) \quad (4)$$

$$g_i(\mathbf{r} + \mathbf{c}_i \Delta t, t + \Delta t) - g_i(\mathbf{r}, t) = -\frac{\Delta t}{\tau_g} (g_i - g_i^{eq}) \quad (5)$$

Hydrodynamic variables are related to above velocity distribution functions by,

$$\rho \equiv \sum_i f_i, \quad \rho v_\alpha \equiv \sum_i c_{i\alpha} f_i, \quad \phi \equiv \sum_i g_i \quad (6)$$

Also,

$$\sum_i f_i^{eq} \equiv \rho, \quad \sum_i c_{i\alpha} f_i^{eq} \equiv \rho h v_\alpha, \quad \sum_i g_i^{eq} \equiv \phi \quad (7)$$

Expressions for equilibrium distribution functions are reported in [1].

4 LB Method and Method of Lines

Equation (3) can be solved using method of lines. In this section, we compare various aspects of algorithms of LB method(LBM) and method of lines(MOL)

Time complexity

Average time required for one iteration in both the algorithms was noted and plotted in Figure 1a. It was noted that time for one iteration of MOL is almost equal to LB method with D2Q9 lattice. Time varies linearly with number of points for both the algorithms. Hence both shows time complexity of $\mathcal{O}(n)$

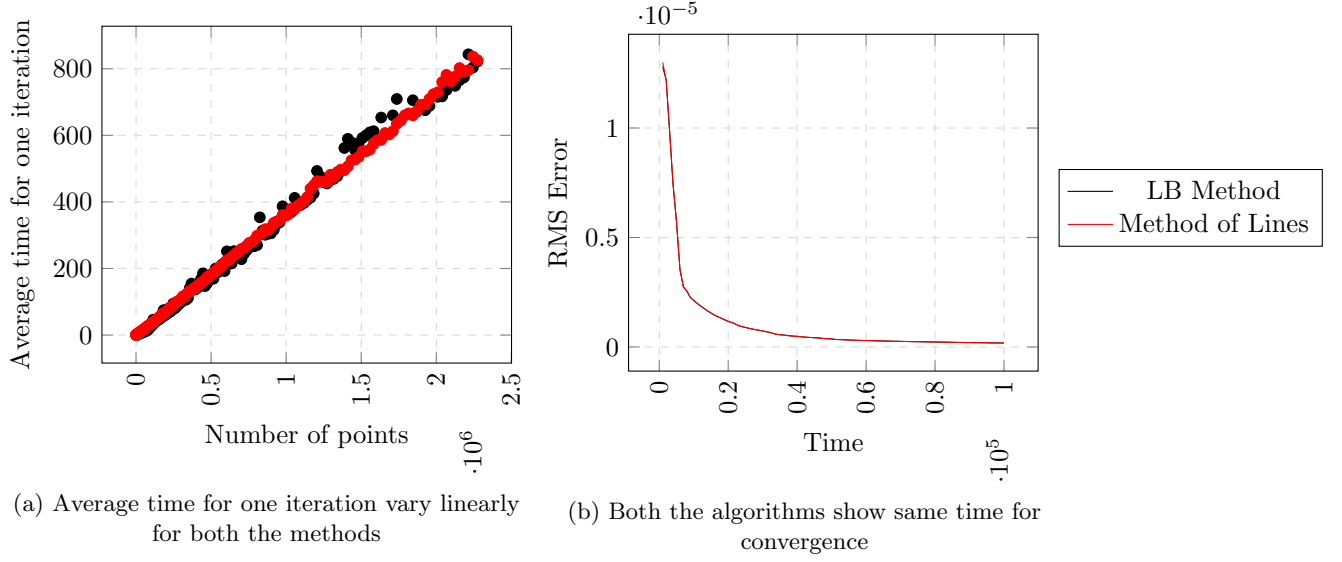


Figure 1: Time complexity and convergence analysis for LB method and method of lines

Space complexity

Both the algorithms have same space complexity $\mathcal{O}(n)$

Time for convergence

It was noted that both the methods gives almost same result and error at a particular time and takes almost same time to converge to a solution.

5 Spinodal decomposition

Spinodal decomposition is a mechanism for the rapid unmixing of a mixture of liquids or solids from one thermodynamic phase, to form two coexisting phases. Refer Figure 2 for the spinodal decomposition simulation where we started with each point having a random ϕ value where $-1 \leq \phi \leq 1$.

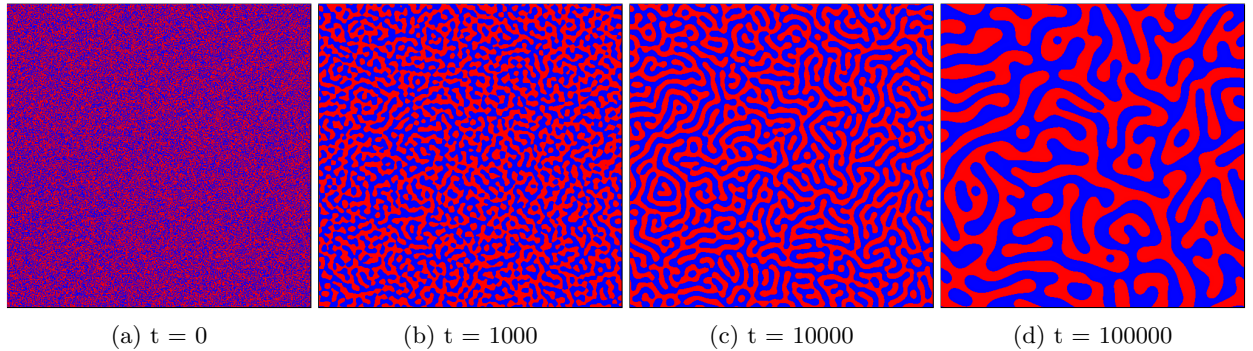


Figure 2: Spinodal decomposition simulation in a domain of 500×500 using Lattice Boltzmann method. It can be seen that phases unmix to form separate clusters.

[Click here to see the video of the simulation.]

6 Surface tension

Surface tension is the elastic tendency of a fluid surface which makes it acquire the least surface area possible. For any volume, sphere gives the least surface area. In the following simulation, a cubic volume of liquid is taken at $t = 0$. As expected, the droplets changes itself to a spherical droplet. (Refer Figure 3)

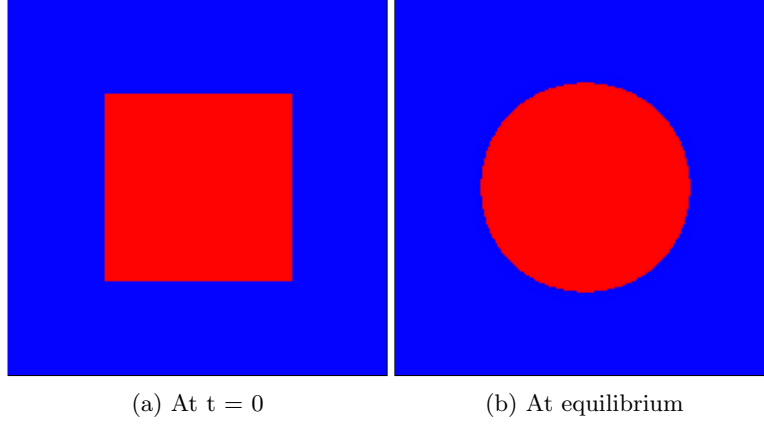


Figure 3: Evolution of a square surface to a circular surface.

7 Variation of phase field close to interfase

Close to interface, the phase field varies as a hyperbolic tangent with the normal coordinates to the interface, r . Simulation data was perfectly matching with the numerical solution given by [2]. (Refer Fig 4)

$$\phi(r) = \phi_{eq} \tanh\left(\frac{r}{\epsilon}\right) \quad (8)$$

where $\phi_{eq} = \sqrt{-a/b}$ and $\epsilon \equiv \sqrt{-2k/a}$ is the interface thickness

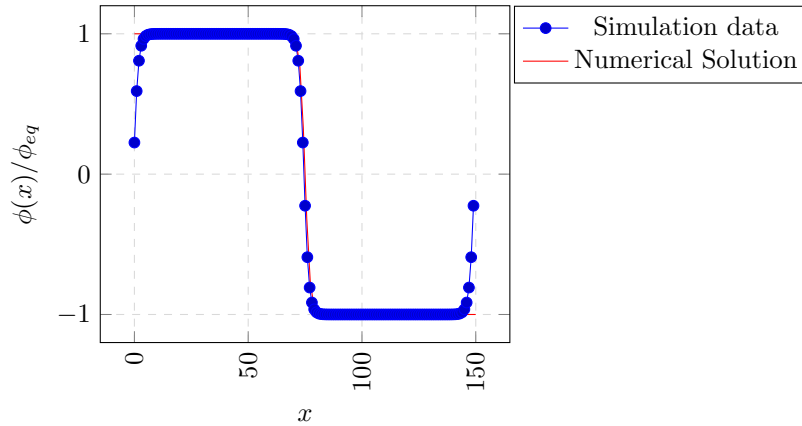


Figure 4: Phase field profile along normal to interface of two already separated phases

8 Solid wall

Bounce-back rules [3] are imposed along the boundary for impenetrability and no-slip boundary conditions. Also,

$$\vec{n} \cdot \nabla \mu = 0 \quad (9)$$

For an equilibrium contact angle on an ideal solid wall, geometrical formulation is used for implementing wetting condition [4, 5].

$$\phi_{i,j,1} = \phi_{i,j,3} + \tanh\left(\frac{\pi}{2} - \theta\right)\xi \quad (10)$$

where

$$\xi = \sqrt{(\phi_{i+1,j,2} - \phi_{i-1,j,2})^2 + (\phi_{i,j+1,2} - \phi_{i,j-1,2})^2} \quad (11)$$

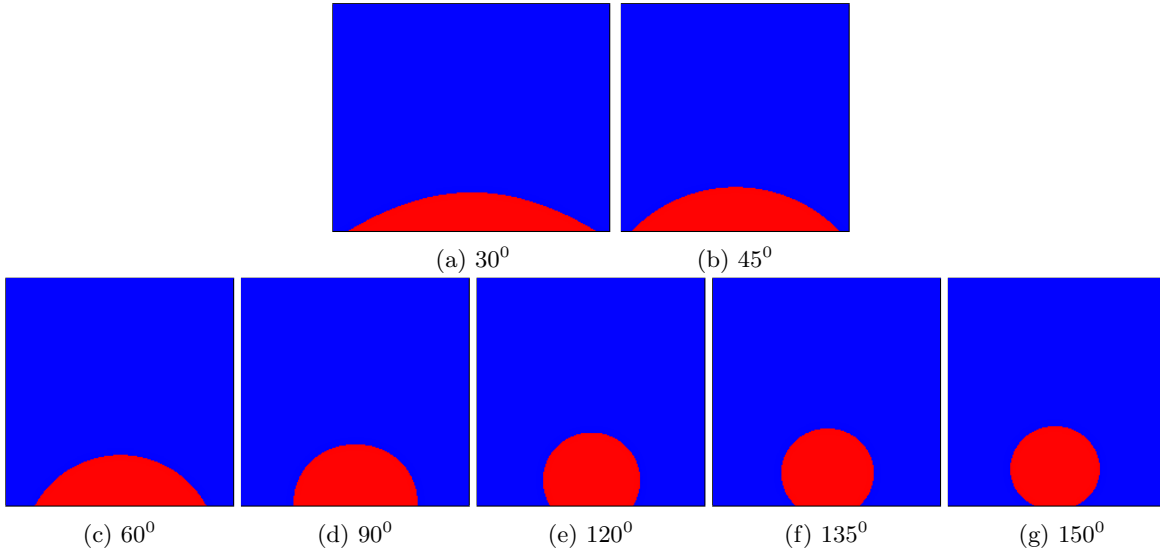


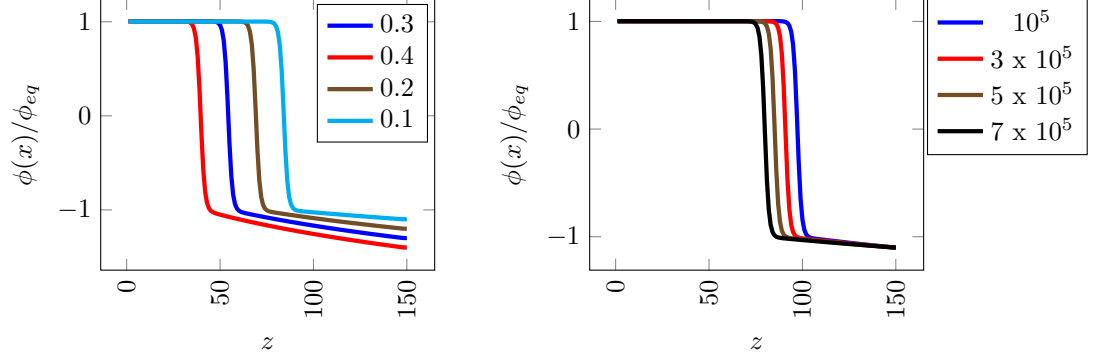
Figure 5: Droplets on solid wall with different contact angles

9 Evaporation of a planar droplet

To drive evaporation of the film we impose the boundary condition $\phi(z = z_H, t) = \phi_H$, where $\phi_H < -\phi_{eq}$. This induces a gradient in the chemical potential field μ . In response to this imbalance, the system reduces ϕ , which corresponds to the evaporation of the film[6]. Phase field imbalance, $\Delta\phi_H \equiv -\phi_{eq} - \phi_H$. We performed simulations in a box consisting of $1 \times 1 \times 150$ lattice sites. Periodic boundary conditions were set in the x and y directions. A wall was located at $z_w = 1$, while the concentration was fixed to a value ϕ_H at $z_H = N_z$ to drive the system out of equilibrium. The initial height of the film was set to $z_0 = 100$.

10 Condensation of planar droplet

Similar to evaporation, condensation can be simulated by imposing boundary condition $\phi(z = z_H, t) = \phi_H$, where $\phi_H > -\phi_{eq}$. In Figure 7, a planar droplet of height 100 is evaporated with $\phi_H = -1.1$. After 5×10^6 timesteps, boundary condition at $z = 150$ is changed to $\phi_H = -0.245$ (at which μ is equal and opposite to that of $\mu(\phi = -1.1)$) to initiate evaporation. It is observed that after condensing for same duration as that of evaporation, at $t = 10 \times 10^6$ the system returns to the initial condition.



(a) After 5×10^6 simulation steps with different ϕ_H

(b) Phase field profile at different time steps

Figure 6: Phase field profile for the planar film evaporation.

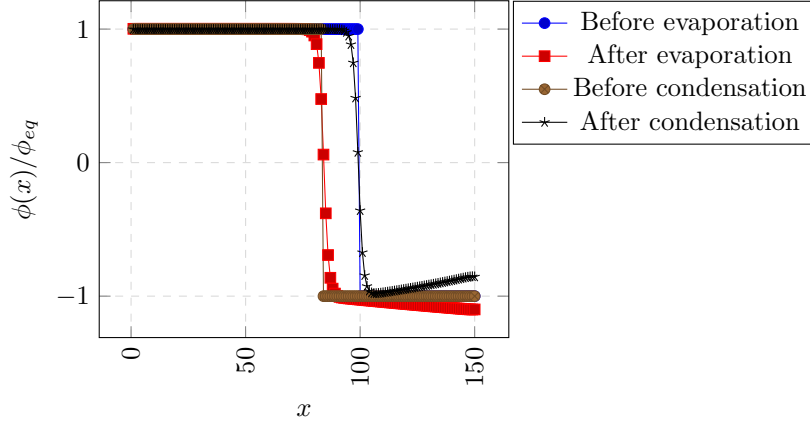


Figure 7: Phase field profile along normal to interface of evaporating and condensing planar droplet.

11 Evaporation and condensation of a sessile droplet on a solid surface

11.1 Ideal surface

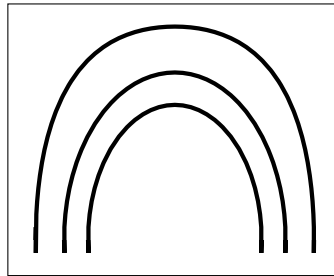


Figure 8: Shape profile of an evaporating droplet on an ideal surface.

An ideal solid surface is flat, rigid, perfectly smooth, and chemically homogeneous, and has zero contact angle hysteresis. On such a surface, only one thermodynamically stable contact angle exists. Hence we expect a constant contact angle and varying contact diameter during evaporation and condensation.

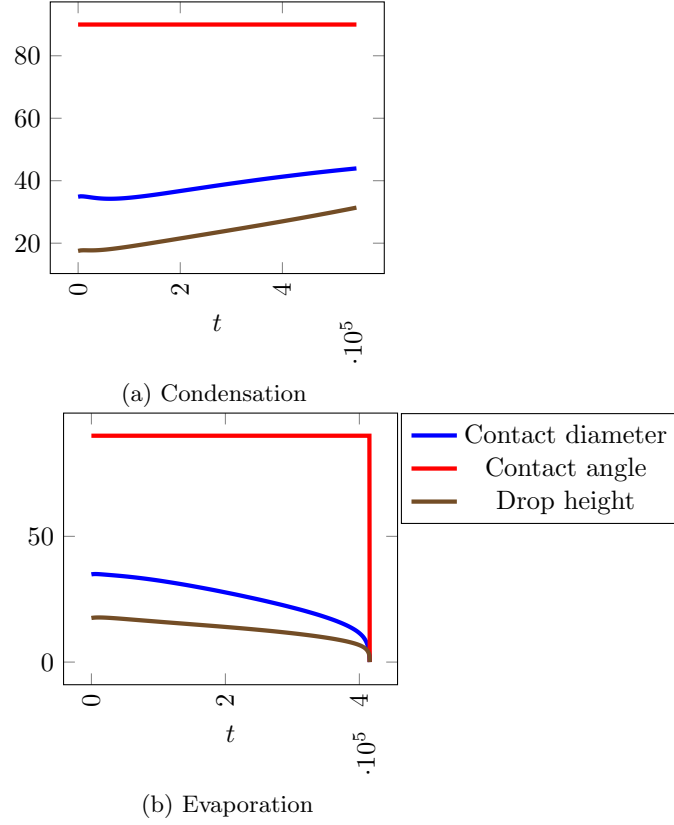


Figure 9: Contact diameter, angle and drop height of a droplet on an ideal surface with equilibrium contact angle 90° during evaporation/condensation.

11.2 Hysteretic surface

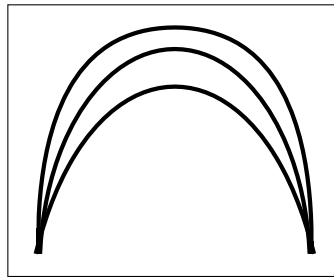


Figure 10: Shape profile of an evaporating droplet on a hysteretic surface.

In many natural systems, the solid walls are usually rough and chemically inhomogeneous. In these surfaces, contact angle hysteresis has to be taken into consideration. Due to hysteresis, the contact line

remains pinned when the local contact angle θ is within a hysteresis window.

$$\theta_R \leq \theta \leq \theta_A \quad (12)$$

where θ_R and θ_A denote the receding angle and advancing angle respectively.

When θ is greater than θ_A , the contact line moves forward. When θ is less than θ_R , the contact line moves backward. To realize this effect, at each time step of computation, we should first obtain the local apparent contact angle at the contact points. Then, comparisons of θ with θ_R and θ_A are required. If $\theta \leq \theta_R$, θ in Eq.11 should be replaced by θ_R ; if $\theta \geq \theta_A$, θ should be replaced by θ_A ; else θ in Eq.11 remains unchanged.

A small difference in contact angle imposed using Eq.11 and measured contact angle was observed in the simulation. This difference was causing error while implementing contact angle hysteresis, i.e, the contact angle θ was reaching θ_R at a very short time causing contact angle pinning to be visible for very small duration. Hence, difference between measured angle and imposed angle was plotted in Figure 11 and this data was used to correct the measured angle.

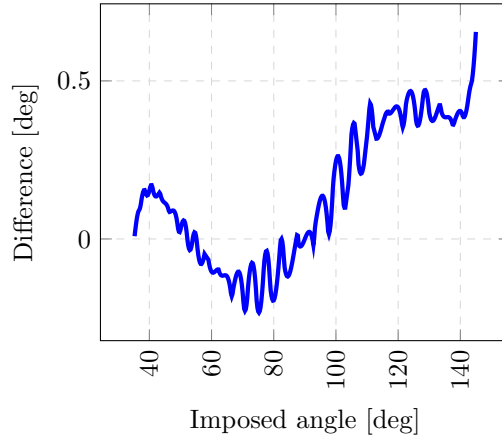


Figure 11: Difference between imposed contact angle and measured contact angle

Picknett and Bexon[7] followed the mass and profile evolution of organic liquid drops. They observed three distinct evaporation modes: mode 1, during which the solid and liquid interface area remains constant (when hysteresis exists); mode 2, for which the contact angle remains constant (ideal system with no hysteresis at equilibrium); mode 3, which is a mixed mode. They also observed that evaporation follows the first mode until $\theta = \theta_R$, and then, the second mode is initiated.[8]

In Figure 12 a droplet with initial contact angle 90° is evaporating on a surface with $\theta_R = 42^\circ$ and $\theta_A = 140^\circ$. It follows mode 1 in the initial stage where contact diameter stays constant whereas contact angle decreases. After contact angle reaches $\theta = \theta_R$, mode 2 is observed in which contact angle stays at θ_R and the contact diameter reduces.

In Figure 13 a droplet with initial contact angle 70° is condensing on a surface with $\theta_R = 42^\circ$ and $\theta_A = 90^\circ$. In the early stage, contact line is pinned (constant contact diameter) as the contact angle increases to θ_A . Once the θ reaches θ_R contact angle stays at θ_A and contact diameter also increases with drop height.

12 Discussion and Conclusions

We discussed two methods for study of evaporation and condensation - Lattice Boltzmann algorithm and Method of lines. Both of the methods show $\mathcal{O}(n)$ time complexity and $\mathcal{O}(n)$ space complexity. Time for one iteration of 4th order Runge Kutta method and LB method on D2Q9 lattice was found to be almost same. Both the methods showed identical error from previous time steps and time for convergence. Lattice boltzmann method was used for rest of the work and is validated by simulating spidodal decomposition, evolution of a square surface into a circular one and studying variation of phase field close to interface.

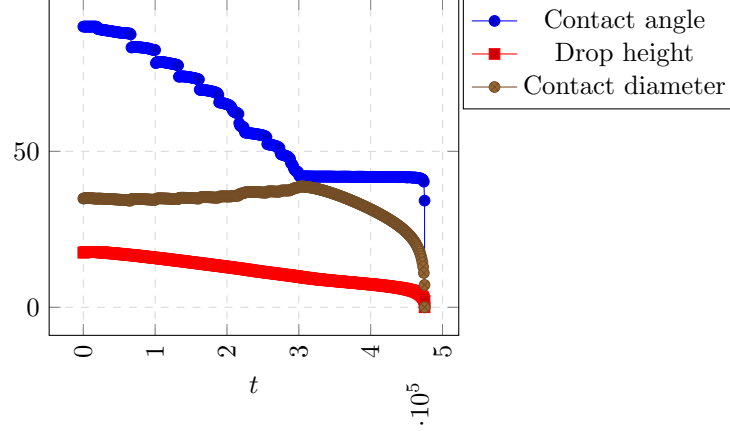


Figure 12: Profile of an evaporating droplet on a hysteretic surface.

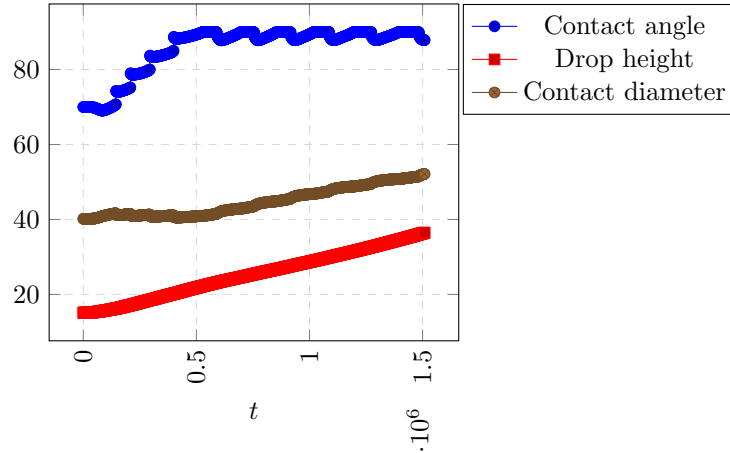


Figure 13: Profile of a condensing droplet on a hysteretic surface.

Evaporation was implemented by imposing a boundary condition $\phi(z = z_H, t) = \phi_H$, where $\phi_H < -\phi_{eq}$. This induces a gradient in the chemical potential field μ . In response to this imbalance, the system reduces ϕ , which corresponds to the evaporation of the film[6]. A reverse effect was observed when boundary condition $\phi(z = z_H, t) = \phi_H$, where $0 > \phi_H > -\phi_{eq}$. Hence we were able to simulate condensation in the system. With equal chemical potential gradient, amount of liquid evaporated was found to be equal to that of condensed (Refer Figure 7).

Wetting condition proposed by H. Ding and P. D. M. Spelt[5] was found to have a difference between imposed and measured angle. It can reduce time in hysteresis window drastically. For correct study of contact angle hysteresis, this should be corrected by mapping measured contact angle to difference between imposed and measured angle. This difference should be added to measured angle as a correction.

Evaporation and condensation was studied on an ideal and non-ideal surface. On an ideal surface during the both process, contact angle stays constant whereas contact diameter and drop height changes. On a hysteretic surface, contact diameter was staying constant until contact angle reaches θ_R or θ_A after which contact angle was staying constant. This result was in accordance with experimental results recorded by Picknett and Bexon[7]. Contact line was pinned when θ is in the hysteresis window. A complete pinning of the contact line can be achieved by imposing $\theta_R = 0^\circ$ or $\theta_A = 180^\circ$.

13 Future work

In this study, we were able to implement contact line pinning along with evaporation. Flow of fluid and particles can be incorporated in this model to study coffee ring effect. While simulating evaporation, a constant driving force was applied on the system. However, in real world this may not be the case. A varying driving force could more accurately model the process.

References

- [1] J.-C. D. I. P. P. B. V. M. Kendon, M. E. Cates, “Inertial effects in three dimensional spinodal decomposition of a symmetric binary fluid mixture: A lattice boltzmann study,” *J. Fluid Mech.* 440 (2001) 147-203, 2000.
- [2] I. P. P.T. Sumesh and R. Adhikari, “Lattice boltzmann - langevin simulations of binary mixtures,” *Phys. Rev. E* 84, 046709 (2011), 2011.
- [3] A. J. C. L. Verberg, “Lattice-boltzmann simulations of particle-fluid suspensions,” *Journal of Statistical Physics*, vol. 104, no. 5, pp. 1191–1251, 2001.
- [4] H.-b. H. Lei Wang and X.-Y. Lu, “Scheme for contact angle and its hysteresis in a multiphase lattice boltzmann method,” *Phys. Rev. E* 87, 013301, 2013.
- [5] H. Ding and P. D. M. Spelt, “Wetting condition in diffuse interface simulations of contact line motion,” *Phys. Rev. E*, vol. 75, p. 046708, Apr 2007.
- [6] R. Ledesma-Aguilar, D. Vella, and J. M. Yeomans, “Lattice-boltzmann simulations of droplet evaporation,” *Soft Matter*, vol. 10, no. 41, pp. 8267–8275, 2014.
- [7] R. Picknett and R. Bexon, “The evaporation of sessile or pendant drops in still air,” *Journal of Colloid and Interface Science*, vol. 61, no. 2, pp. 336 – 350, 1977.
- [8] C. Bourges-Monnier and M. E. R. Shanahan, “Influence of evaporation on contact angle,” *Langmuir*, vol. 11, no. 7, pp. 2820–2829, 1995.